

Triboresistive Touch Sensing: Grid-Free Touch-Point Recognition Based on Monolayered Ionic Power Generators

Younghoon Lee, Sungsoo Lim, Won Jun Song, Sudong Lee, Sohee John Yoon, Jae-Man Park, Min-Gyu Lee, Yong-Lae Park, and Jeong-Yun Sun*

Recent growing pursuit of skin-mountable devices has been impeded by the complicated structures of most sensing systems, containing electrode grids, stacked multilayers, and even external power sources. Here, a type of touch sensing, termed “triboresistive touch sensing”, is introduced for gridless touch recognition based on monolayered ionic power generators. A homogeneous monolayer, i.e., ionic poly(dimethylsiloxane) (PDMS), generates electricity based on the electric field generated by touch. Voltages generated at each corner of the ionic PDMS rely on resistance between touch points and each corner, ensuring recognition of the touch positions without the need for electrode grid layers and external power sources. With notable advantages of high transparency (96.5%), stretchability (539.1%), and resilience (99.0%) of the ionic PDMS, epidermal triboresistive sensing is demonstrated to express touch position and readily play a musical instrument. A gridless system of triboresistive sensing allows rearrangement of the touch sections according to a given situation without any physical modification, and thus easily completes consecutive missions of controlling position, orientation, and gripping functions of a robot.

been applied more closely to the human body. Owing to the soft and curved nature of human skin, the systems need to be flexible, robust, and transparent to ensure operational reliabilities and to provide comforts.^[3,4] However, it has been challenging to ensure these desirable properties due to the complicated structures of conventional touch-sensing systems, which contain a network of individual electrodes and stacked multilayers.^[4,5,8,10,12] More importantly, sensing systems inevitably rely on external power sources, which potentially sacrifice flexibility, add weight, and decrease the lifetime of the sensing systems.^[4,5,8,12–14]

To address the issues originated from the use of external power sources, systems that rely on energy-harvesting technologies have been highlighted as an alternative to conventional touch-sensing systems.^[3,15–17] Recently, triboelectric

1. Introduction

The advent of wireless sensor networks has inspired rapid development of detection systems for seamless interaction with electronic devices.^[1–3] In particular, touch-sensing systems based mostly on the principles of capacitive^[4–7] and piezoresistive^[8–11] touch-sensing mechanisms, have played important roles in diverse electronic devices. Recently, to communicate information accurately and conveniently, sensing systems have


nanogenerators (TEGs), which convert mechanical touch to electrical energy, have been developed to provide a platform for touch-sensing capability that does not rely on additional power sources.^[16–20] The self-powered touch-sensing capability of TENGs can be realized with a couple of materials, i.e., a dielectric layer attached to a conducting layer, based on the combined effects of contact electrification and electrostatic induction.^[3,17,18,21] To ensure that triboelectric touch sensors are skin-mountable, researchers have worked to make the components stretchable and transparent. Soft materials such as poly(dimethylsiloxane) (PDMS) and ionically conductive gels are suitable for use in skin-mountable triboelectric touch sensors thanks to their high transparency, stretchability, resilience, and easily tunable mechanical properties.^[17,22–25]

Nonetheless, the development of triboelectric touch position sensors with reliable stretchability and transparency remains challenging due to the complicated structures of the sensors, which contain multiple stacked layers and arrays of individual electrodes.^[16,17,19,21,26,27] Unfortunately, the stacking process deteriorates the outstanding mechanical/optical properties of the soft materials in TENGs since the sensors require an additional conducting layer of a material such as metal, ceramic, carbon materials, etc.^[16,28–30] The inclusion of transparent and stretchable materials like gels also results in easy delamination and blurring at the bonding interfaces.^[17,19,31] Relying on a complex array of individual electrodes and corresponding wires

Y. Lee, S. Lim, W. J. Song, J.-M. Park, M.-G. Lee, J.-Y. Sun
 Department of Materials Science and Engineering
 Seoul National University
 Seoul 08826, Republic of Korea
 E-mail: jysun@snu.ac.kr

Y. Lee, S. Lee, S. J. Yoon, Y.-L. Park
 Department of Mechanical Engineering
 Seoul National University
 Seoul 08826, Republic of Korea

J.-Y. Sun
 Research Institute of Advanced Materials (RIAM)
 Seoul National University
 Seoul 08826, Republic of Korea

 The ORCID identification number(s) for the author(s) of this article can be found under <https://doi.org/10.1002/adma.202108586>.

DOI: 10.1002/adma.202108586

worsens deformability of the sensors. The deformability can be limited by an unstable interface originating from the different elastic moduli of the materials and poor interfacial adhesion. The bonding interface may also cause diffraction of light, which harms the transparency of the sensor. Furthermore, under applied deformation, the grid will get inhomogeneous spacing, resulting in a loss of sensing resolution. To address the challenges, if triboelectric touch sensors can be operated without relying on complicated structures, the scope of application of such sensors would expand greatly.

Here, we introduce a type of sensing mechanism for grid-free touch recognition based on monolayered ionic power generators, which we call “triboresistive touch sensing”. To realize a triboresistive touch sensor, ionic PDMS was designed to have ability to conduct ions without sacrificing its transparency and stretchability. The ion conduction capability allowed the monolayered ionic PDMS to generate electrical energy based on the electric field induced by touch. Using the power generated by touch, we explored a triboresistive touch sensing without depending on additional electrode grid layers and external power sources.

2. Results and Discussion

2.1. Conventional TENG Touch Sensors and Triboresistive Touch Sensors

To generate electrical energy based on contact electrification and electrostatic induction, structure of conventional TENGs have been basically required to be formed by stacking a couple of layers, containing dielectric and conducting layers (Figure 1a).^[3,17,18,32] The integration of an electrode grid layer allows a TENG to detect touch positions as well. However, to secure the resolution of touch position sensing, a complicated electrode grid and corresponding data line connections are required. Furthermore, under a deformation, the grid will get inhomogeneous spacing, resulting in a loss of the sensing resolution. To address these challenges, we explored grid-free touch recognition based on monolayered ionic power generators. (Figure 1b; the design of an ionic PDMS is shown in greater detail in Figure 2). The introduction of ions in a dielectric layer (i.e., PDMS in this work) endows the PDMS with the capacity for electrostatic induction without requiring an additional conducting layer. Ions in the PDMS can act as charge carriers instead of conducting layers to induce current (Figure S1, Supporting Information). Touching an ionic PDMS can generate voltages, which can be directly utilized to detect the position of the touch. The difference in voltage generated at each corner, which relies on resistance between the touch points and each corner, ensures that the sensor can recognize touch positions without depending on electrode grid layers, the corresponding measurement tools, or external power sources (the working mechanism is discussed in detail in Figures 4 and 5).

2.2. Ionic PDMS Design

PDMS is a promising material in the field of wearable devices, particularly in the field of TENG, and it is well known as one of

the representative hydrophobic materials. On the other hand, ionic liquid (IL)-which is hydrophilic-is known to be a useful conductive material. The key challenge in the design of an ionically conductive elastomer is obtaining homogeneous mixtures of polymer and IL. Our approach to achieve stability is both to adjust the polarity of both intrinsically hydrophobic PDMS and hydrophilic IL and to promote strong bonding interactions such as hydrogen bonding^[33–38] and ion–dipole interactions.^[39–42] In particular, hydrogen bonding (H-bonding), which is a unique type of dipole–dipole interaction between molecules, has been highlighted due to its notable strength. The strength of H-bonding allows homogeneous mixing compatibility, thus avoiding the loss of generation^[36] and the issue of leakage.^[37] There are two types of hydrogen bonding, which are known as red-shift and blue-shift hydrogen bonding.^[43] The red-shift is known as strong H-bonding. To promote red-shifted H-bonding, specific strong dipole units (X–H, where X is a highly negative atom such as N, O, or F) as the H-bonding donor are added to a polar polymer. On the other hand, the use of specific dipole units limits the applicability of this approach to many promising polymers for ionically conductive elastomers, such as PDMS. PDMS lacks certain exact functional groups such as hydroxyl group, so its capacity for H-bonding is limited. To overcome the challenges associated with the design of ionic PDMS, we adopted to the introduction of hydroxyl group into PDMS as a means of inducing H-bonding with ionic liquid.

To elaborate, there are three approaches that can be used to design ionic PDMS: (1) enhancing the hydrophilicity of PDMS by using a polar functional group, (i.e., ester and hydroxyl group), to enable hydrophilization of PDMS, thus resulting in strong interactions with IL. And enhancing the hydrophobicity of the IL by (2) Investigating the effect of alkyl chain length on the cationic part, and (3) changing the anionic part to compatibility with an innately hydrophobic PDMS species. Prior studies have verified the effects of various anionic part of IL on miscibility.^[38,39] Thus, we focused on the first two approaches of (1) and (2). We conducted a simple mixing test with functionalized PDMS and [EMIM]⁺[TFSI][−] to attempt to identify candidate PDMS. (See the section entitled “The strategies of designing the ionic PDMS” and “The effect of functional groups in PDMS on mixing with [EMIM]⁺[TFSI][−] in the Supporting Information.)

As shown in Figure S2 (Supporting Information), we attempted to identify the most suitable PDMS (i.e., DMS-U21) which is capable of H-bonding with IL through the introduction of targeted functional groups. We expected our system to be fully stabilized through H-bonding between the –OH group in DMS-U21 and the –CF₃ group in bis(trifluoromethanesulfonyl) imide ([TFSI][−]) in IL. However, we found that the mixtures of DMS-U21 and [EMIM]⁺[TFSI][−] were not fully homogenous or sufficiently translucent. Thus, it was necessary to design an additional interaction to obtain fully homogeneous mixtures of DMS-U21 containing IL. Reportedly, as the concentration of the alkyl chain in imidazolium base IL increases, local dynamic heterogeneities are observed.^[44,45] These local dynamic heterogeneities between alkyl chains in IL are induced by van der Waals interactions when the number of alkyl chain carbons exceeds 6.^[44] We assume that the nano-domains separated by

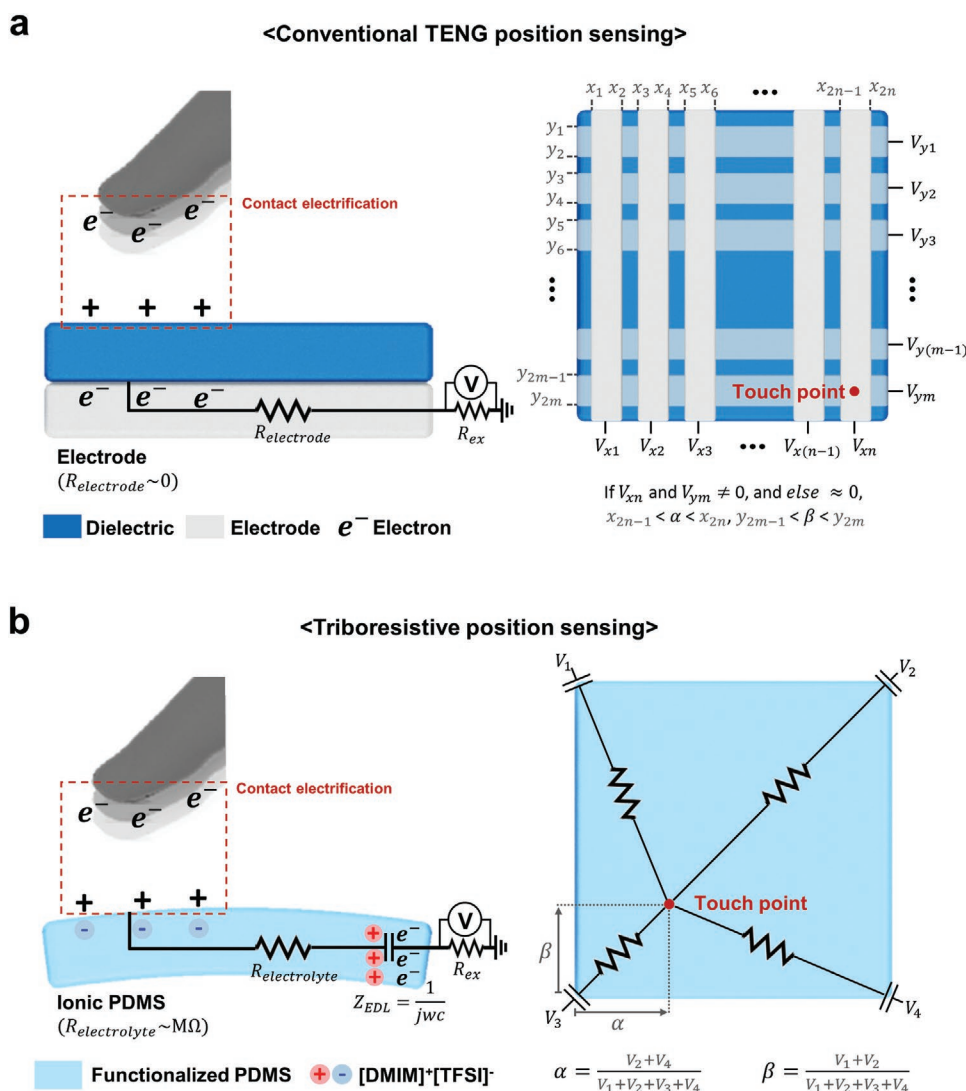


Figure 1. Working mechanisms of conventional triboelectric nanogenerators (TENGs) position sensing and triboresistive position sensing. a) Conventional TENGs are basically composed of multiple layers, including a dielectric layer and an electrode for contact electrification and electrostatic induction. To detect a touch position, the conventional sensors must be assembled with complicated electrode grids. b) An ionic PDMS is designed to address the need for both contact electrification and electrostatic induction. Ions in the PDMS act as charge carriers without an additional electrode layer. The difference in voltages generated at each corner, which relies on the resistance between the touch points and each corner, allows the sensor to recognize touch positions without depending on an electrode grid layer or an external power source.

alkyl chains in $[C_n\text{MIM}]^+[\text{TFSI}]^-$ may have induced van der Waals interactions with dimethyl siloxane units in PDMS to enhance the compatibility with DMS-U21.

To identify this assumption, we arranged three candidate PDMS with four kinds of 1-alkyl-3-methylimidazolium bis(trifluoromethanesulfonyl)imide ($[C_n\text{MIM}]^+[\text{TFSI}]^-$, $n = 2, 4, 6$, and 12) with different alkyl chain lengths (n), which are 1-ethyl-3-methyl-imidazolium bis(trifluoromethanesulfonyl)imide ($[\text{EMIM}]^+[\text{TFSI}]^-$ or $[\text{C}_2\text{MIM}]^+[\text{TFSI}]^-$), 1-butyl-3-methyl-imidazolium bis(trifluoromethanesulfonyl)imide ($[\text{BMIM}]^+[\text{TFSI}]^-$ or $[\text{C}_4\text{MIM}]^+[\text{TFSI}]^-$), 1-hexyl-3-methyl-imidazolium bis(trifluoromethanesulfonyl)imide ($[\text{HMIM}]^+[\text{TFSI}]^-$ or $[\text{C}_6\text{MIM}]^+[\text{TFSI}]^-$) and 1-dodecyl-3-methyl-imidazolium bis(trifluoromethanesulfonyl)imide ($[\text{DMIM}]^+[\text{TFSI}]^-$ or $[\text{C}_{12}\text{MIM}]^+[\text{TFSI}]^-$) in Figure 2a. As shown by the photographs

and magnified optical spectroscopic images in Figure 2b, we prepared three compounds and each of which consists of: (i) Sylgard184, (ii) DMS-R11, (iii) DMS-U21 blended with 10 vol% $[\text{DMIM}]^+[\text{TFSI}]^-$. As a result, only one combination, (iii) DMS-U21 mixed with 10 vol% $[\text{DMIM}]^+[\text{TFSI}]^-$, showed clear and transparent images. Phase separation was observed in both (i) Sylgard 184 and (ii) DMS-R11 blended with $[\text{DMIM}]^+[\text{TFSI}]^-$. When a strong interaction exists (i.e., H-bonding), the domains segregated by alkyl chains in $[\text{DMIM}]^+[\text{TFSI}]^-$ assist in improving the degree of compatibility between the polymer and IL by introducing van der Waals interactions. Additionally, we measured the optical properties by UV-vis transmittance and the hydrophilicity by static contact angle (SCA), as shown in Figure S3 (Supporting Information). At a wavelength of 550 nm, the transmittance spectra of DMS-U21, DMS-R11,

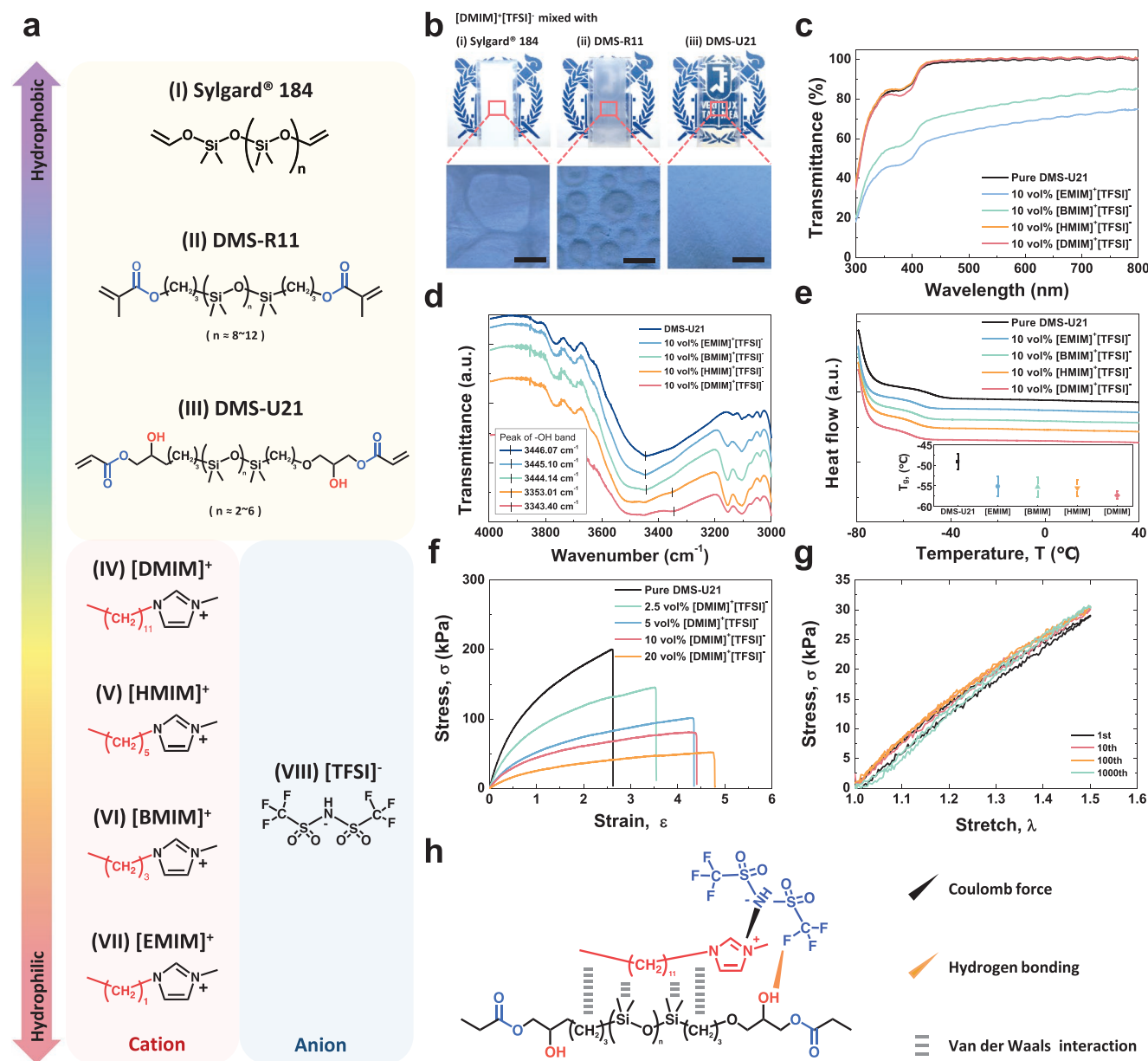


Figure 2. Ionic PDMS design concept. a) Chemical structures of the PDMS family: (i) Sylgard 184; (ii) methacryloxypropyl-terminated poly(dimethylsiloxane) (DMS-R11); (iii) (3-acryloxy-2-hydroxypropoxypropyl)-terminated poly(dimethylsiloxane) (DMS-U21). The series of 1-alkyl-3-methylimidazolium ([C_nMIM]⁺) ($n = 2, 4, 6$, and 12): (iv) 1-dodecyl-3-methylimidazolium ([DMIM]⁺); (v) 1-hexyl-3-methylimidazolium ([HMIM]⁺); (vi) 1-butyl-3-methylimidazolium ([BMIM]⁺); (vii) 1-ethyl-3-methylimidazolium ([EMIM]⁺). (viii) Bis(trifluoromethanesulfonyl)imide ([TFSI]⁻) is a pair of a series of [C_nMIM]⁺. b) Photographs and magnified images of each type of PDMS mixed with 10 vol% of [DMIM]⁺[TFSI]⁻. Phase separation was rarely observed, as shown in the magnified image in (iii). Scale bar: 50 μm. c) UV-vis spectra of pure DMS-U21 and DMS-U21 mixed with [C_nMIM]⁺[TFSI]⁻. The transmittance of DMS-U21 mixed with [DMIM]⁺[TFSI]⁻ was 99% at a wavelength of 550 nm. d) FT-IR spectra of pure [DMIM]⁺[TFSI]⁻, pure DMS-U21, and DMS-U21 containing 10 vol% of [C_nMIM]⁺[TFSI]⁻ ($n = 2, 4, 6$, and 12). For pure DMS-U21, the band located at 3446.07 cm⁻¹ is assigned to stretching of the -OH group. Upon [C_nMIM]⁺[TFSI]⁻ ($n = 6$ and 12) was added, the H-bonded -OH band occurs at a lower wavenumber. As the number of carbon on alkyl chain of [C_nMIM]⁺[TFSI]⁻ is increased from 6 to 12, the H-bonded -OH bands are shifted gradually from 3353.01 to 3342.40 cm⁻¹. e) Differential scanning calorimetry (DSC) traces of pure DMS-U21 and the mixture of DMS-U21 and 10 vol% of [C_nMIM]⁺[TFSI]⁻. The glass transition temperature (T_g) of DMS-U21 decreased from -49.1 to -57.3 °C as the length of the alkyl chain of [C_nMIM]⁺[TFSI]⁻ increased. f) Tensile stress-stretch curves of DMS-U21 mixed with [DMIM]⁺[TFSI]⁻. The concentration of [DMIM]⁺[TFSI]⁻ ranged from 0 to 20 vol% in DMS-U21. The stretch (λ) is defined by the distance of sample when the sample is deformed. g) Stress-stretch curves of DMS-U21 mixed with 10 vol% [DMIM]⁺[TFSI]⁻ during 1000 cycles of loading-unloading under applied stretch of 1.5. The linear elastic behavior was observed, and it indicated good resilience of DMS-U21 mixed with 10 vol% [DMIM]⁺[TFSI]⁻. h) Chemical structure illustrating possible interactions between DMS-U21 and [DMIM]⁺[TFSI]⁻.

and Sylgard 184 containing 10 vol% [DMIM]⁺[TFSI]⁻ were 96.5%, 59.4%, and 9.7%, respectively. Furthermore, the SCA, which was measured with deionized water (DW) and pure

[DMIM]⁺[TFSI]⁻, decreased as more hydrophilic functional groups, such as ester and hydroxyl groups, were introduced to the PDMS. Thus, the results support the notion that a longer

alkyl chain on imidazolium affects the degree of compatibility between DMS-U21 and $[\text{DMIM}]^+[\text{TFSI}]^-$.

We further investigated the evidence of H-bonding and the effect of the alkyl chain length of imidazolium on miscibility with DMS-U21 using UV-vis spectroscopy, Fourier transform infrared (FT-IR) spectroscopy, and differential scanning calorimetry (DSC). As the number of carbons in the alkyl chain of $[\text{C}_n\text{MIM}]^+$ increased, the tendency of transmittance of the mixtures of DMS-U21 and $[\text{C}_n\text{MIM}]^+[\text{TFSI}]^-$ approached 96.5% at 550 nm (Figure 2c). When DMS-U21 was blended with $[\text{HMIM}]^+[\text{TFSI}]^-$ or $[\text{DMIM}]^+[\text{TFSI}]^-$, the transmittance of each mixture was comparable to that of pure DMS-U21. However, the transmittance was lowered to 76.8% and 66.5% when $n \leq 4$ in $[\text{C}_n\text{MIM}]^+$ (i.e., $[\text{BMIM}]^+$ and $[\text{EMIM}]^+$, respectively).

As shown in Figure 2d, while the characteristic stretching bend located at 3446.07 cm^{-1} was assigned to the $-\text{OH}$ functional group in pure DMS-U21, $-\text{OH}$ functional group was not assigned in $[\text{C}_n\text{MIM}]^+[\text{TFSI}]^-$ (Figure S4, Supporting Information). Upon the addition of $[\text{C}_n\text{MIM}]^+[\text{TFSI}]^-$ ($n = 2, 4, 6$, and 12), the assigned $-\text{OH}$ group at 3446.07 cm^{-1} shifted weakly to lower wavenumber. Particularly, as the number of carbon on alkyl chain of $[\text{C}_n\text{MIM}]^+[\text{TFSI}]^-$ is increased from 6 to 12, a band of the H-bonded $-\text{OH}$ group not only are occurred at lower wavenumber but also are lowered gradually from 3353.01 to 3342.40 cm^{-1} . The stretching band of $-\text{CF}_3$ group (1194.35 cm^{-1}) was shifted to higher wavenumber upon the addition of $[\text{C}_n\text{MIM}]^+[\text{TFSI}]^-$ ($n = 2, 4, 6$, and 12) in Figure S5 in the Supporting Information. Accordingly, the shift of bands indicates the formation of H-bonding between H-bonding donor ($-\text{OH}$) and H-bonding acceptor ($-\text{CF}_3$).

We concluded that the presence of a longer alkyl chain in $[\text{C}_n\text{MIM}]^+$ supported the compatibility of DMS-U21 and $[\text{C}_n\text{MIM}]^+[\text{TFSI}]^-$ due to van der Waals interactions. Furthermore, plasticizing effect of IL in ionic PDMS was observed from DSC. As shown in Figure 2e, the glass transition temperature (T_g) of each sample was lowered from -46.0 to $-57.3\text{ }^\circ\text{C}$ upon the addition of 10 vol% $[\text{C}_n\text{MIM}]^+[\text{TFSI}]^-$ in accordance with the increase in alkyl chain length. This proved that length of the alkyl chain in imidazolium is critical for the degree of miscibility with DMS-U21.

The presence of an appropriate plasticizing effect induced by IL was confirmed by the results of the uniaxial tensile test. By tuning the volume ratio of ionic liquid ($[\text{DMIM}]^+[\text{TFSI}]^-$) to polymer (DMS-U21), a series of complex materials with improved compatibility and distinct mechanical properties were obtained. The sample fabrication processes and a magnified cross-sectional image of the ionic PDMS are described in the Experimental Section and Figure S6 in the Supporting Information, relatively.

As shown in Figure 2f, upon increasing the content of $[\text{DMIM}]^+[\text{TFSI}]^-$ up to 20 vol%, the material showed lower Young's modulus, greater stretchability, and lower maximum fracture stress. The Young's modulus and critical stretch at rupture (λ_c) of 10 vol% $[\text{DMIM}]^+[\text{TFSI}]^-$ samples are summarized in Figure S7 in the Supporting Information. In comparison with Sylgard 184 elastomer, the Young's modulus was lower, in the range of $223.1\text{--}26.8\text{ kPa}$, while the critical stretch (λ_c) was in the range of $3.7\text{--}5.9$, making the material sufficiently adaptable to skin due to softening of the samples through the plasticizing

effect. In addition, all samples exhibited a transmittance of greater than 96% under a wide range of $[\text{DMIM}]^+[\text{TFSI}]^-$ concentrations from 2.5 to 20 vol% (Figure S8, Supporting Information).

The 10 vol% $[\text{DMIM}]^+[\text{TFSI}]^-$ ionic PDMS exhibited various hysteresis behaviors under applied stretch of 1.5–4 on the loading–unloading test (Figure S9a, Supporting Information). Additionally, the plastic strain ratio was calculated by the ratio of residual strain ($\epsilon_{\text{residual}}$) to applied strain ($\epsilon_{\text{applied}}$) and plotted as a function of the number of cycles in Figure S9b in the Supporting Information. We figured out that the 10 vol% $[\text{DMIM}]^+[\text{TFSI}]^-$ ionic PDMS exhibited highly resilient behavior for stretch below 2. Specifically, in the 1000-cycle loading–unloading test, full recovery was observed at applied stretch of 1.5, as the sample immediately returned to its original status; this is shown in Figure 2g. Notably, the average resilience during the 1000 cycles was 99.0%.

As illustrated in Figure 2h, the compound with DMS-U21 and $[\text{DMIM}]^+[\text{TFSI}]^-$ is exhibited with plausible interactions, including H-bonding and van der Waals interactions. The components are thoroughly homogeneous, thus indicating highly transparent with no phase separation. H-bonding are induced by introduction of the hydroxyl group on PDMS and the anion in IL. Further, the van der Waals interactions are confirmed by the filling of the alkyl chains on imidazolium in IL with dimethylsiloxane units.

2.3. Power Generation by an Ionic PDMS

Ions dissolved in the ionic PDMS act as a medium to transmit electric field instead of additional conducting layers. The suggested power generation mechanism of ionic PDMS is described in detail in Figure S1 in the Supporting Information. To experimentally investigate the power generation capability of ionic PDMS, a pushing tester was used to provide consistent vertical contacts (see the Experimental Section and Figure S10 in the Supporting Information for details). As shown in Figure 3a, when bare PDMS was touched, a negligible amount of voltage was generated due to the absence of a conducting layer, causing poor electrostatic induction. To endow the PDMS with electrostatic induction capability without inserting an additional conducting layer, ions can be introduced into the PDMS, as described in Figure S1 in the Supporting Information. $[\text{DMIM}]^+[\text{TFSI}]^-$ was introduced at up to 10 vol%. The generated voltage was dramatically increased about 61 times. The stable addition of $[\text{DMIM}]^+[\text{TFSI}]^-$ allowed the PDMS to act as not only a dielectric layer for contact electrification but also an ion conducting layer for electrostatic induction. Meanwhile, the addition of further ionic liquid from 10 to 20 vol% caused the generated voltage to decrease, which is possibly a result of reduced contact electrification capability due to a decrease in the PDMS content. The effect of $[\text{DMIM}]^+[\text{TFSI}]^-$ on contact electrification was investigated in Figure S11 in the Supporting Information.

The effect of thickness on voltage generation was investigated, as shown in Figure 3b and Figure S12 (Supporting Information). A conventional TENG device composed of $50\text{ }\mu\text{m}$ -thick PDMS assembled on a conducting layer generated

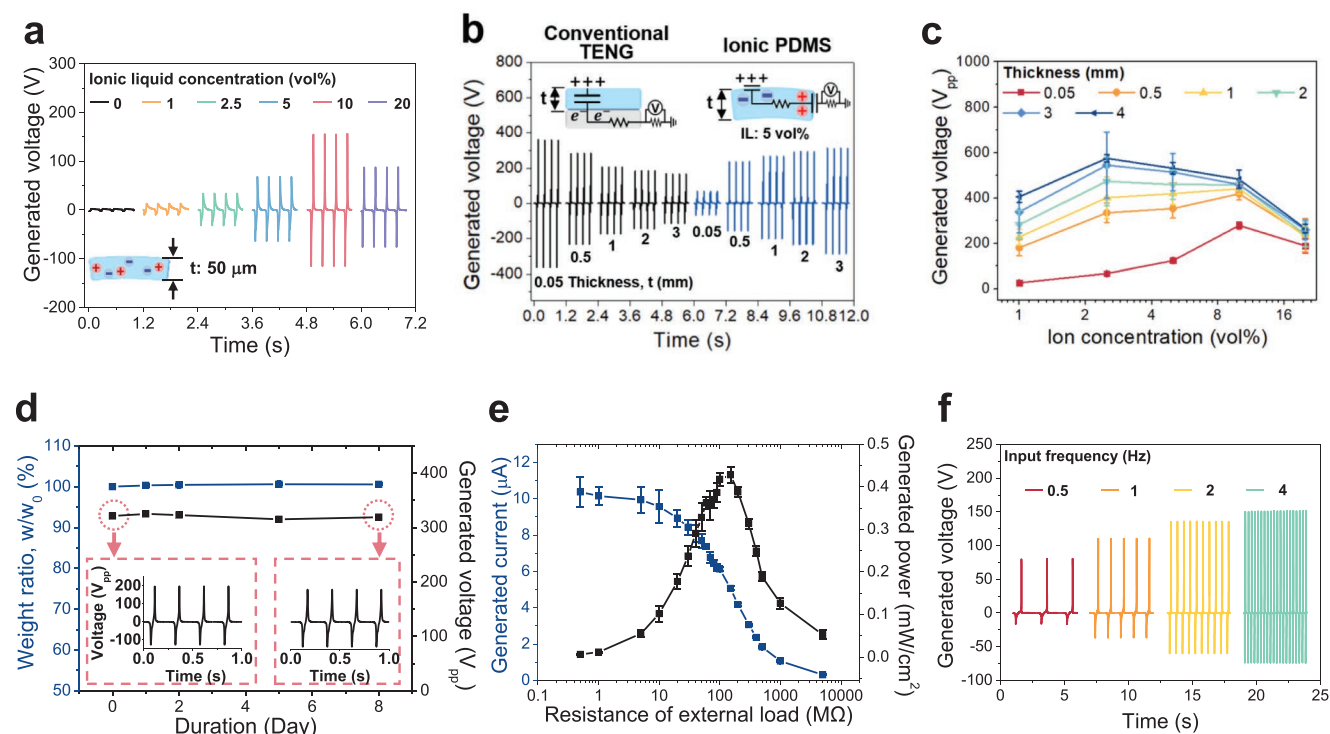


Figure 3. Characterization of power generation in an ionic PDMS. a) Generated voltages under various ionic liquid concentrations from 0 to 20 vol% in the PDMS. PDMS with 0 vol% ionic liquid generated negligible voltages. b) Voltage generation of an ionic PDMS and a conventional TENG was measured as the thickness of each sample increased from 50 μm to 3 mm. The PDMS used in the conventional TENG and the ionic PDMS was DMS-U21. c) The effect of thickness on generated voltages was investigated under various ion concentrations from 0 vol% to 20 vol%. d) The durability of the ionic PDMS was investigated for 8 days. Insets are the generated voltages of the ionic PDMS on the first day and after 8 days. e) Generated currents and powers of the ionic PDMS under various external loads. f) Generated voltages under various contact frequencies from 0.5 to 4 Hz. All the error bars in the figure represent the standard error of the mean.

a voltage of 735 V_{pp} , which is markedly higher than the voltages generated by the ionic PDMS. However, increasing the thickness of the PDMS from 50 μm to 3 mm decreased the voltage generation from 735 to 285 V_{pp} . An electric field from an object is transmitted to a conducting layer through the PDMS.^[46–48] If the PDMS becomes thicker, then the electric field transmitted to the conducting layer is diminished, resulting in decreased voltage generation across an external load. On the other hand, the ionic PDMS does not depend on a conducting layer to transmit an electric field to an external load, as the electric field is transmitted through ion conduction in the ionic PDMS.^[35,49] Ionic conductance can be enhanced if the PDMS becomes thicker, resulting in increased voltage generation across an external load. As a result, when the thickness of ionic PDMS was increased from 50 μm to 3 mm, the generated voltage notably rose from about 135 to 610 V_{pp} .

The effect of thickness on the generated voltage was investigated under various ionic liquid concentrations from 1 to 20 vol% (Figure 3c). When the thickness of ionic PDMS was micrometer-scale, the maximum power generation occurred at an ion concentration of 10 vol%. On the other hand, as the thickness of ionic PDMS approached the millimeter scale, the maximum voltage generation point was shifted to lower ion concentration of 2.5 vol%. Optimum voltage generation depending on coupling effect of ion concentration and thickness is discussed in Figure S13 in the Supporting Information

in detail. The findings indicate that thickness and ionic concentration can be optimized according to each particular application.

There have been numerous attempts to realize transparent and stretchable TENGs.^[15,17,19,50–52] Among them, the strategy of introducing a gel as a conducting layer has been spotlighted. However, researchers have been struggling to deal with the evaporation of solvent from the gels, which results in poor durability. Compared to a conventional TENG based on a gel conducting layer, ionic PDMS is free from volatile solvent and still remains both transparent and stretchable. As shown in Figure 3d, after 8 days in a harsh condition of a vacuum, the weight of the ionic PDMS was negligibly changed and its voltage generation capability at the initial state was maintained. Furthermore, in accordance of the H-bonding, the leaking issue of IL on the ionic PDMS are confirmed via Squeezing test in Figure S14 (Supporting Information) and the voltage generation capacity rarely degraded during 50000 consecutive contacts in Figure S15 in the Supporting Information. To investigate the maximum power generation of the ionic PDMS, generated current was measured under a wide range of external loads from 0.5 $M\Omega$ to 5 $G\Omega$ (Figure 3e; Figure S16, Supporting Information). At an external load of 150 $M\Omega$, the ionic PDMS generated a maximum power of 0.43 mW cm^{-2} . The peak of generated power can be affected by contact speed. The generated voltage gradually decreased as the contact frequency decreased from 4 to 0.5 Hz (Figure 3f). However, a notable voltage of 98 V_{pp} was

still measured at 0.5 Hz. The output performances of an ionic PDMS contacting with various types of materials were investigated in Figure S17 in the Supporting Information. Gentle touch readily generated electrical energy ($\approx 68 V_{pp}$) and directly turned on nine green LEDs connected in series (Figure S18 and Movie S1, Supporting Information).

2.4. Triboresistive Touch Sensing

As shown in Figure 4a and Figure S19 (Supporting Information), we suggest triboresistive touch sensing based on gridless ionic power generators. Based on the power generation mechanism explained in Figure S1 (Supporting Information), the ionic PDMS can be directly utilized for touch position recognition by comparing the generated voltages measured on each side. The internal parts of the ionic PDMS can be expressed as two resistive parts from the touch point to each side. The induced voltages at each voltmeter are inversely proportional to the resistance. The induced voltages can be represented by the following equations

$$V_1 \approx \frac{R_2 + R_{ex}}{R_1 + R_2 + 2R_{ex}} R_{ex} I_t = (1 - \alpha) I_t R_{ex} \quad (1)$$

$$V_2 \approx \frac{R_1 + R_{ex}}{R_1 + R_2 + 2R_{ex}} R_{ex} I_t = \alpha I_t R_{ex} \quad (2)$$

where V_1 and V_2 are the peak-to-peak induced voltages measured by voltmeter V_1 and V_2 , respectively; I_t is the total induced current; R_1 and R_2 are the resistances between the touch point and each side, respectively; R_{ex} is the total resistance of the external load and voltmeter; and α is the normalized distance from the touch point to left end of the ionic PDMS. The derivations of Equations (1) and (2) are described in detail in Figure S19 (Supporting Information) and the section entitled “Triboresistive sensing mechanism of a strip-type sensor” in the Supporting Information. The positions can be interpreted based on the following equation

$$\alpha = \frac{V_2}{V_1 + V_2} \quad (3)$$

Seven positions on the ionic PDMS with an 8.8 mm gap distance between each point were touched, and the generated voltages were measured by voltmeters V_1 and V_2 (Figure 4b; Figure S20, Supporting Information). Because the ionic PDMS is intrinsically stretchable, the sensing capability was also investigated after it was stretched by up to 50%. The induced voltages corresponding to each touch position are shown in Figure 4c. The voltages measured on each side were inversely proportional to the distance from the touch position. During touches TP#1 to TP#7, the voltages induced at V_1 decreased and the voltages induced at V_2 increased based on Equations (1) and (2), respectively. When TP#4 was touched, similar voltage

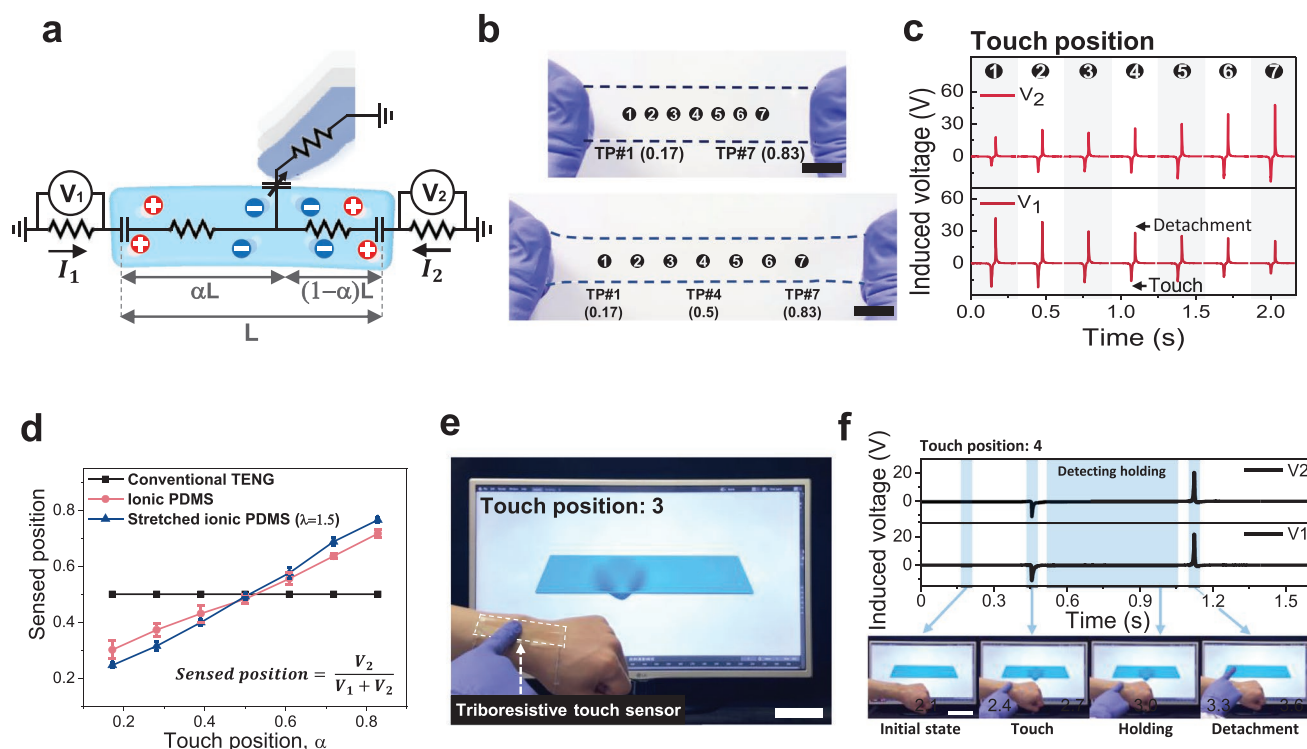


Figure 4. Triboresistive touch-sensing strip. a) Equivalent electrical circuit of the triboresistive sensing strip. b) Photographs of the triboresistive sensing strip in the initial state and after being stretched by 50%. To demonstrate the position sensing capability of the sensor, seven touch positions (TP#1 to TP#7) were investigated. Scale bar: 1 cm. c) When the positions from TP#1 to TP#7 were touched, the induced voltage was measured by voltmeters (V_1 and V_2) connected to both ends of the sensor. d) The generated voltages were used to calculate the sensed position. The sensing capability in the initial state and after being stretched (50%) were compared to the sensing capability of the conventional TENG. e) A photograph of an epidermal triboresistive touch sensor detecting touch position. Scale bar: 5 cm. f) The triboresistive sensor is capable of detecting holding as well as touching and detaching. Scale bar: 8 cm. All the error bars in the figure represent the standard error of the mean.

levels were induced at each voltmeter, indicating that the center of the ionic PDMS was touched. Based on Equation (3), the touch position was translated to the sensed position, as shown in Figure 4d. Even though some distortion was observed, the calculated sensed position traced the touch position (α) during touches TP#1 to TP#7. Based on Equations (1) and (2), the distortion most likely occurred because the induced voltage is not only affected by R_1 and R_2 , but also by R_{ex} . Moreover, nonlinearity of conduction path in the ionic PDMS and contact resistance at the interfaces of the connected wires possibly result in some distortion.^[14,42] Thanks to the softness of the ionic PDMS, the sensing capability of the ionic PDMS could be investigated under stretched states. When the PDMS was stretched by up to 50%, the sensing capability was maintained; the distortion was even suppressed compared to that in the undeformed state (Figure 4d; Figure S21a, Supporting Information). Meanwhile, the conventional TENG could not be used for the suggested triboresistive sensing mechanism because extremely low resistance (10^4 to 10^7 S m⁻¹)^[2,22,53] of the conventional conducting layer caused the ratio of R_1 and R_2 to total resistance to be negligible (Figure S21b, Supporting Information). The spatial resolution of the triboresistive touch sensor was investigated (Figure S22, Supporting Information). The strip type of the ionic PDMS was touched every 1 mm. The touch position distances of 1 mm were readily distinguished with a sensitivity (S) of 0.009 mm⁻¹ (see Figure S22 in the Supporting Information for details). Considering that the width of the human fingertip is ≈ 20 mm,^[54] the ability to distinguish touches within less than 1 mm can be considered in practice to be a highly reliable spatial resolution for touch sensors.

Because the suggested triboresistive touch-sensing mechanism relies on the ratio of voltages induced on each side, the magnitude of the generated voltage barely affects the sensing capability (Figure S23, Supporting Information). Thanks to the softness of the ionic PDMS, it could be attached to a wrist with adhesive and easily deformed along with movement of the wrist (see Experimental Section and Figure S24 (Supporting Information) for details). Moreover, the high transmittance of the ionic PDMS ensured that visual information could be conveyed through the ionic PDMS. The ionic PDMS mounted on the skin readily recognized touch positions from TP#1 to TP#7 (Figure 4e; Movie S2, Supporting Information). Because direction of voltages induced by touch is opposite compared to voltages induced by detach, the sensor readily perceived touch and detach movements. Holding could be also detected until the detaching signal was received (Figure 4f; Movie S2, Supporting Information). Integration with future applications such as playing the piano was also demonstrated (Figure S25 and Movie S3, Supporting Information). Furthermore, based on the properties described above, future direction for the multi-touch detection was discussed in Figure S26 in the Supporting Information.

2.5. A Triboresistive Touch Sensor for Control of a Robot

The ionic PDMS was directly utilized as a controller to manipulate a robot (Figure S27, Supporting Information). While the touch resolution of conventional TENG touch position sensors

is limited by the number of arrays, the resolution of the suggested triboresistive sensor is determined by the relative voltages induced at each corner, resulting in high and flexible touch resolution. As described in Figure 5a and Figures S28 and S29 (Supporting Information), the ionic PDMS was divided into nine sections to control the movements of a robot, including the position and gripping functions of the robot. Thanks to the flexible resolution of the sensor, the sections could be readily rearranged according to a given situation without any physical modification of the ionic PDMS. After rearranging the sensing sections from nine to seven sections of irregular arrangement, orientation including roll, pitch, and yaw of the robot could be controlled as well. The voltages induced at each corner were measured when the sixteen sections were touched (Figure S30, Supporting Information). To demonstrate the use of an epidermal triboresistive touch sensor as a controller, a sensor was attached to the back of a hand and connected with four wires (Figure 5b). The induced voltages were notably distinguishable according to touch sections, and could be interpreted to command sixteen movements of the robots (Movie S4, Supporting Information). The triboresistive touch sensor was used to control a robot as the robot gripped a leaning egg and conveyed it to a target spot (Figure 5c,d; Figures S31 and S32 and Movie S5, Supporting Information). When a section near V_2 was touched and held, both α and β were over 0.6, which commanded the robot to “Move down” (i). To grip the egg, a section near V_3 was touched and held. The presence of a clear detach signal avoided breaking the egg (ii) (Figure S31, Supporting Information). After delicately gripping the egg, the robots moved the egg up, which was done in response to the signals $\alpha < 0.4$ and $\beta > 0.6$ (iii). To stand the leaning egg up, the “Next page” section was touched (iv). The area and functions of each section were rearranged to allow the subject to manipulate the robot's orientation. After rolling the egg by touching the rearranged section near V_3 (v), the egg was delicately conveyed to a target spot. Finally, the upright egg was released with a touch in the middle between V_3 and V_4 , which corresponded to a signal of $\alpha \approx 0.5$ and $\beta < 0.4$ (vi). The sampling rate of the triboresistive touch sensor was about 1 kHz, which was enough for sufficiently delicately control of the robots, as 150–200 ms is the minimum period for humans to perceive visual changes (Figure S33, Supporting Information).^[55]

Some slight sensing distortion was observed, which may have originated from unstable wire connections and the nonlinearity of the conduction path in the ionic PDMS,^[14,42] but an improved calibration process may be able to compensate for such distortion.

3. Conclusion

A triboresistive sensing is suggested for grid-free touch recognition based on ionic power generators. By employing hydrogen bonding and van der Waals interactions with [DMIM]⁺[TFSI]⁻, an intrinsically homogeneous ionic PDMS exhibiting high transmittance (96.5%), stretchability (539.1%), resilience (99.0%), and ionic conductivity (0.25 mS m⁻¹) was designed to generate power based on the electric field generated by touch. The stable introduction of 10 vol% [DMIM]⁺[TFSI]⁻ into the

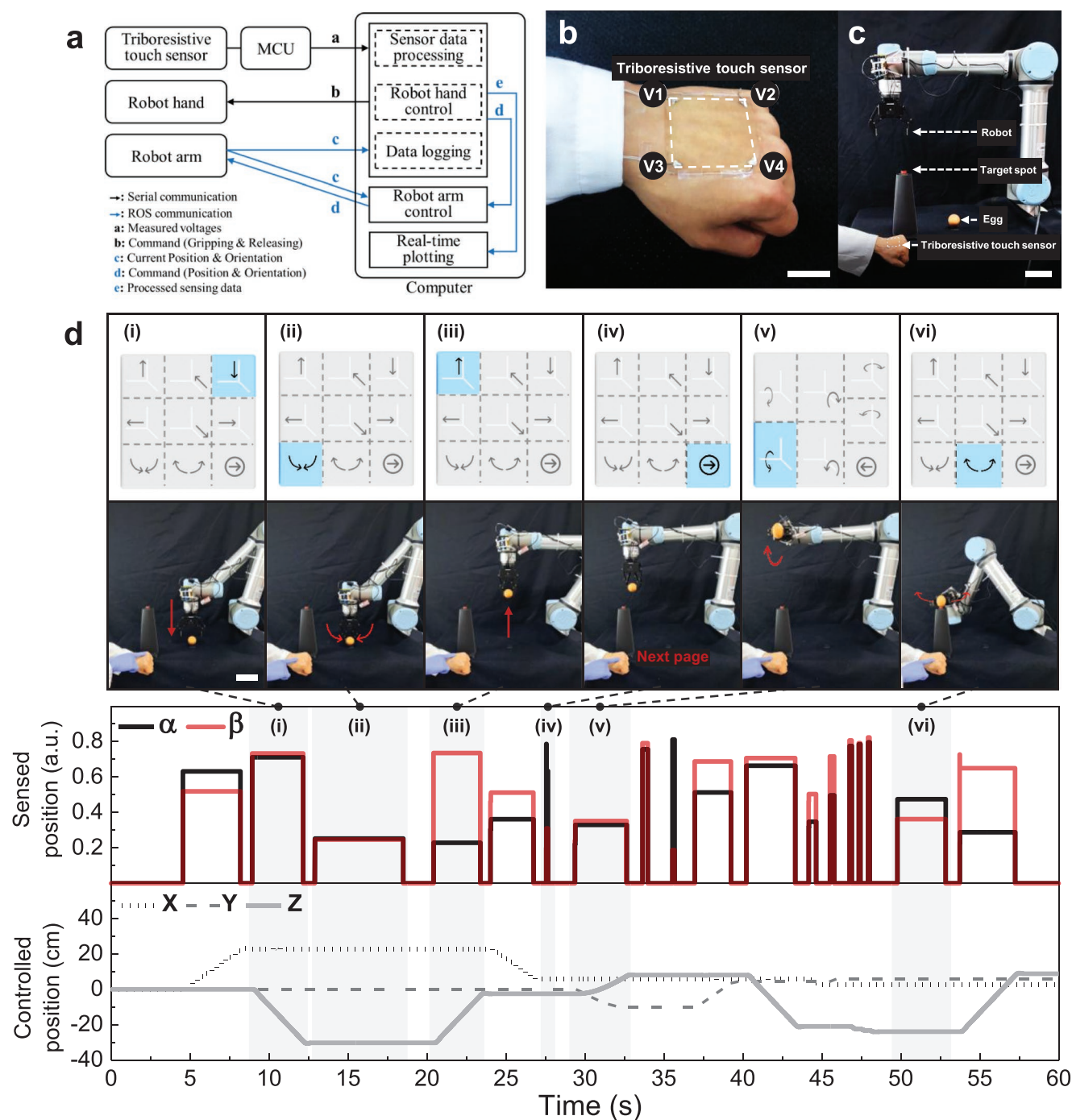


Figure 5. Tribore sistive controller for manipulation of a robot hand and arm. a) Block diagram describing communication between the tribore sistive touch sensor and the robot. b) The tribore sistive touch sensor was attached to the back of a hand. Each corner of the ionic PDMS was connected with wires to a microcontroller unit (MCU). Scale bar: 2 cm. c) The robot was connected to the sensor to demonstrate precise control of the robot's position, orientation, gripping, and releasing. Scale bar: 8 cm. d) Demonstration of control of the robot with various motions including "Move down" (i), "Grip" (ii), "Move up" (iii), "Next page" (iv), "Decrease roll" (v), "Release" (vi), etc. Scale bar: 8 cm.

PDMS enabled the ionic PDMS to generate electrical energy up to 268 V_{pp}, which is 61 times higher than that of PDMS without ion introduction.

The power generated by touch on the ionic PDMS was directly utilized to detect touch position by measuring the electric potential at each corner. A comparison of the voltages

generated at each corner, which depend on the resistance between the touch points and each corner, allows for estimation of the touch positions without the need for electrode grid layers and external power sources. The tribore sistive sensor was used to express touch position, play a musical instrument, and control a robot. Tribore sistive sensing opens up exciting

opportunities for broader applications in the realm of next-generation tactile sensors, wearable human-machine interfaces, and soft robotics.

4. Experimental Section

Materials: (3-Acryloxy-2-Hydroxypropoxypropyl)-terminated poly(dimethylsiloxane) (DMS-U21, Gelest), methacryloxypropyl-terminated poly(dimethylsiloxane) (DMS-R11, Gelest), and poly(dimethylsiloxane) (Sylgard 184, Dow Corning) were used as base materials. 1-Ethyl-3-methylimidazolium bis(trifluoromethanesulfonyl)imide ([EMIM]⁺[TFSI]⁻; E0599, TCI), 1-butyl-3-methylimidazolium bis(trifluoromethanesulfonyl)imide ([BMIM]⁺[TFSI]⁻; B2477, TCI), 1-hexyl-3-methylimidazolium bis(trifluoromethanesulfonyl)imide ([HMIM]⁺[TFSI]⁻; H1423, TCI), and 1-dodecyl-3-methylimidazolium bis(trifluoromethanesulfonyl)imide ([DMIM]⁺[TFSI]⁻; D5694, TCI) were used as charge carriers. Pentaerythritol tetrakis(3-mercaptopropionate) (PETMP; 381 462, Sigma-Aldrich) was used as a crosslinker with DMS-U21 for thiol-ene reactions. Benzoin ethyl ether (BEE; 172 006, Sigma-Aldrich) was used as a photoinitiator. All chemicals were used as received without further purification. An acrylic adhesive (VHB; F9460PC, 3M) was used as double-sided tape. A platinum electrode was used to measure the electrical characteristics of the ionic PDMS, and silver-coated copper wire was used to create the electrical circuit.

Specimen Preparation: The method for preparing a series of ionic PDMS was as follows: 3 mL of DMS-U21, 333 μ L of [C_nMIM]⁺[TFSI]⁻ ($n = 2, 4, 6$, and 12), 737.5 μ L of PETMP and 20 μ L of 0.1 M BEE were dissolved in acetone. Each precursor solution was mixed with a 5 mL Luer lock syringe (5 mL All Plastic Syringe, Luer tip; A5, Norm-ject). Then, the mixtures were poured into a prepared poly(1,1,2,2-tetrafluoroethylene) (PTFE; ASF-110FR, CHUKOH)-covered slide glass substrate. The molded solution was cured in two steps: with heat (60 °C) in an oven for one day, then with ultraviolet light for 2 h (8 W power and 365 nm wavelength at 50 °C). After the curing step, acetone was removed by placing the sample in a desiccator for 6 h. The method of preparing a series of DMS-R11 specimens was: 3 mL DMS-R11, 333 μ L [C_nMIM]⁺[TFSI]⁻ ($n = 2$, and 12), and 20 μ L of 0.1 M BEE were dissolved in acetone. The precursor solution was poured into a PTFE-coated glass substrate. The molded solution was cured with ultraviolet light for 2 h (8 W power and 365 nm wavelength at 50 °C). After the curing step, acetone was removed by placing the sample in a desiccator for 6 h. The Sylgard-184-based specimen was prepared by molding a mixture of 2.7 mL base, 0.27 mL curing agents, and 333 μ L [C_nMIM]⁺[TFSI]⁻ ($n = 2$, and 12) followed by heat treatment in a 60 °C oven for one day. The sample designed for attachment to skin was molded on a 500 μ m acrylic adhesive (VHB) substrate.

Mechanical Measurement: For the tensile and loading-unloading tests, the fabricated specimens were cut into strips (30 mm in overall length, 10 mm in width, 1 mm in thickness, and 5 mm in gauge length) using a laser cutter (VLS 3.50, Universal Laser System). The specimens were mounted onto the holding grips of a universal testing machine (3343, Instron) with a 1 kN capacity load cell. All mechanical tests, including the tensile test and loading-unloading cycle test, were performed at room temperature. The stretch rates were fixed at 2 min⁻¹.

Electrical Measurements: The electrical voltage and current of the ionic PDMS were measured by an oscilloscope (DPO5104B, Tektronix) with a voltage probe (TPP0850, Tektronix) and a low-noise current preamplifier (SR570, Stanford Research Systems), respectively. A pushing tester (ET-139, Labworks Inc.), which created consistent vertical contacts, was used to characterize the triboelectric performance. PTFE attached to aluminum film was used as a contact material. Unless otherwise indicated, measurements were performed at room temperature under a gap distance of 2 cm and a frequency of 4 Hz. Measurements were performed after about 1000 precontacts to obtain a stable electrical signal. The resistance of the specimens was measured by a potentiostat (Reference 600+, Gamry). To demonstrate the conversion of mechanical

touch to electrical energy on human skin, VHB was used, both to attach the ionic PDMS to human skin and as an insulating material. A PTFE-coated glove was used as the contact material. All experiments on the human skin were reviewed and approved by Committee of Institutional Review Board (IRB), Seoul National University; the project number is No. 2109/003-005. The volunteer took part with informed consent.

Characterization: Fourier transform infrared spectra (VERTEX 80v, BRUKER) were analyzed to investigate the differences in miscibility between each ionic liquid (i.e., [C_nMIM]⁺[TFSI]⁻, ($n = 2, 4, 6$, and 12)) and PDMS (i.e., Sylgard 184, DMS-R11, and DMS-U21). To investigate the hydrophobicity of each PDMS sample, the contact angles of deionized water and [DMIM]⁺[TFSI]⁻ microdroplets on the specimens were measured using a contact angle analyzer (Smart drop, FEMTOFEB) at room temperature. The average values of three measurements at difference positions on the sample were used. To verify the glass transition temperature (T_g) of ionic PDMS, a DSC (Discovery DSC, TA instrument) experiment in a heating-cooling cycle was conducted. Specimens were placed in a nonhermetic pan, and an empty pan was used as a reference. All of the specimens were first heated from -80 to 120 °C at 10.0 °C min⁻¹, flash frozen to -80 °C, and then heated from -80 to 120 °C at 10.0 °C min⁻¹, and the thermal transitions for the heating cycle were recorded. T_g was determined by the average of the inflection points in the 1st and 2nd heat capacity cycles. A stereomicroscope (Stereo Discovery V12, Zeiss) was used to observe the surface morphology of the fabricated ionic PDMS.

Controlling Robots: The robot consisted of a robot hand (RH-P12-RN, Robotis) and a robot arm (UR5e, Universal Robots). A micro controller unit (MCU) and a computer were used to measure and calculate touch signals. The MCU received voltages generated from corners of the sensor at 800 Hz. These voltages were used to estimate touch position and touch holding using the algorithm presented in Figure S29 in the Supporting Information. As shown in Figure 5a, we controlled the position and orientation of the robot arm through robot operating system (ROS). Gripping functions of the robot hand were controlled by serial communication.

Supporting Information

Supporting Information is available from the Wiley Online Library or from the author.

Acknowledgements

This work was supported by the Materials and Components Technology Development Program of MOTIE/KEIT [10052783] and National Research Foundation of Korea (NRF) grants funded by the Korean Government (Nos. 2018M3A7B4089670, 2021R1C1C2009703, 2021R1A2C2092737). The institute of Engineering Research at Seoul National University provided research facilities for this work.

Conflict of Interest

The authors declare no conflict of interest.

Author Contributions

Y.L. and S.Lim contributed equally to this work. Y.L. and S.Lim conceived of the idea and designed the experiments. S.Lim, Y.L., and J.-M.P. contributed to materials fabrication and characterization. Y.L., S.Lim, W.J.S., and M.-G.L. performed electrical properties characterization and worked on the sensor demonstrations. S.Lee, S.J.Y., and Y.-L.P. developed the program that enabled interaction between the fabricated device and

computer. Y.L. and S.Lim wrote the main manuscript. J.-Y.S. supervised the study and provided intellectual and technical guidance. All authors discussed the results and commented on the manuscript.

Data Availability Statement

The data that support the findings of this study are available from the corresponding author upon reasonable request.

Keywords

ionic elastomers, stretchable ionics, triboelectric nanogenerators, triboresistive touch sensing

Received: October 26, 2021

Revised: February 22, 2022

Published online: March 31, 2022

- [1] X. Liu, J. Liu, S. Lin, X. Zhao, *Mater. Today* **2020**, 36, 102.
- [2] M. D. Dickey, *Adv. Mater.* **2017**, 29, 1606425.
- [3] Y. Lee, W. Song, J.-Y. Sun, *Materials Today Phys.* **2020**, 15, 100258.
- [4] J. Y. Sun, C. Keplinger, G. M. Whitesides, Z. Suo, *Adv. Mater.* **2014**, 26, 7608.
- [5] N. Bai, L. Wang, Q. Wang, J. Deng, Y. Wang, P. Lu, J. Huang, G. Li, Y. Zhang, J. Yang, *Nat. Commun.* **2020**, 11, 209.
- [6] J. Yang, D. Tang, J. Ao, T. Ghosh, T. V. Neumann, D. Zhang, E. Piskarev, T. Yu, V. K. Truong, K. Xie, *Adv. Funct. Mater.* **2020**, 30, 2002611.
- [7] C. B. Cooper, K. Arutselvan, Y. Liu, D. Armstrong, Y. Lin, M. R. Khan, J. Genzer, M. D. Dickey, *Adv. Funct. Mater.* **2017**, 27, 1605630.
- [8] S. Lee, A. Reuveny, J. Reeder, S. Lee, H. Jin, Q. Liu, T. Yokota, T. Sekitani, T. Isoyama, Y. Abe, *Nat. Nanotechnol.* **2016**, 11, 472.
- [9] G. Yun, S.-Y. Tang, S. Sun, D. Yuan, Q. Zhao, L. Deng, S. Yan, H. Du, M. D. Dickey, W. Li, *Nat. Commun.* **2019**, 10, 1300.
- [10] L. Pan, A. Chortos, G. Yu, Y. Wang, S. Isaacson, R. Allen, Y. Shi, R. Dauskardt, Z. Bao, *Nat. Commun.* **2014**, 5, 3002.
- [11] C. L. Choong, M. B. Shim, B. S. Lee, S. Jeon, D. S. Ko, T. H. Kang, J. Bae, S. H. Lee, K. E. Byun, J. Im, *Adv. Mater.* **2014**, 26, 3451.
- [12] M. S. Sarwar, Y. Dobashi, C. Preston, J. K. Wyss, S. Mirabbasi, J. D. W. Madden, *Sci. Adv.* **2017**, 3, e1602200.
- [13] J. T. Muth, D. M. Vogt, R. L. Truby, Y. Mengüç, D. B. Kolesky, R. J. Wood, J. A. Lewis, *Adv. Mater.* **2014**, 26, 6307.
- [14] C.-C. Kim, H.-H. Lee, K. H. Oh, J.-Y. Sun, *Science* **2016**, 353, 682.
- [15] H. J. Kim, B. Chen, Z. Suo, R. C. Hayward, *Science* **2020**, 367, 773.
- [16] Y. C. Lai, H. W. Lu, H. M. Wu, D. Zhang, J. Yang, J. Ma, M. Shamsi, V. Vallem, M. D. Dickey, *Adv. Energy Mater.* **2021**, 11, 2100411.
- [17] Y. Lee, S. H. Cha, Y.-W. Kim, D. Choi, J.-Y. Sun, *Nat. Commun.* **2018**, 9, 1804.
- [18] V. Vallem, Y. Sargolzaeiaval, M. Ozturk, Y. C. Lai, M. D. Dickey, *Adv. Mater.* **2021**, 33, 2004832.
- [19] X. Pu, M. Liu, X. Chen, J. Sun, C. Du, Y. Zhang, J. Zhai, W. Hu, Z. L. Wang, *Sci. Adv.* **2017**, 3, e1700015.
- [20] Y. Lee, W. J. Song, Y. Jung, H. Yoo, M.-Y. Kim, H.-Y. Kim, J.-Y. Sun, *Sci. Rob.* **2020**, 5, eabg9203.
- [21] J. Luo, Z. Wang, L. Xu, A. C. Wang, K. Han, T. Jiang, Q. Lai, Y. Bai, W. Tang, F. R. Fan, *Nat. Commun.* **2019**, 10, 5147.
- [22] C. Keplinger, J.-Y. Sun, C. C. Foo, P. Rothmund, G. M. Whitesides, Z. Suo, *Science* **2013**, 341, 984.
- [23] C. Yang, Z. Suo, *Nat. Rev. Mater.* **2018**, 3, 125.
- [24] T. Wallin, J. Pikul, R. Shepherd, *Nat. Rev. Mater.* **2018**, 3, 84.
- [25] S.-H. Jeong, Y. Lee, M.-G. Lee, W. J. Song, J.-U. Park, J.-Y. Sun, *Nano Energy* **2021**, 79, 105463.
- [26] J. Xiong, P. Cui, X. Chen, J. Wang, K. Parida, M.-F. Lin, P. S. Lee, *Nat. Commun.* **2018**, 9, 4280.
- [27] T. Jin, Z. Sun, L. Li, Q. Zhang, M. Zhu, Z. Zhang, G. Yuan, T. Chen, Y. Tian, X. Hou, *Nat. Commun.* **2020**, 11, 5381.
- [28] H. Wang, M. Shi, K. Zhu, Z. Su, X. Cheng, Y. Song, X. Chen, Z. Liao, M. Zhang, H. Zhang, *Nanoscale* **2016**, 8, 18489.
- [29] D. Jang, Y. Kim, T. Y. Kim, K. Koh, U. Jeong, J. Cho, *Nano Energy* **2016**, 20, 283.
- [30] G. Jian, Q. Meng, Y. Jiao, F. Meng, Y. Cao, M. Wu, *Nanoscale* **2020**, 12, 14160.
- [31] T. Liu, M. Liu, S. Dou, J. Sun, Z. Cong, C. Jiang, C. Du, X. Pu, W. Hu, Z. L. Wang, *ACS Nano* **2018**, 12, 2818.
- [32] F.-R. Fan, Z.-Q. Tian, Z. L. Wang, *Nano Energy* **2012**, 1, 328.
- [33] V. Amoli, J. S. Kim, E. Jee, Y. S. Chung, S. Y. Kim, J. Koo, H. Choi, Y. Kim, D. H. Kim, *Nat. Commun.* **2019**, 10, 4019.
- [34] B. Yiming, Y. Han, Z. Han, X. Zhang, Y. Li, W. Lian, M. Zhang, J. Yin, T. Sun, Z. Wu, *Adv. Mater.* **2021**, 33, 2006111.
- [35] H. J. Hwang, J. S. Kim, W. Kim, H. Park, D. Bhatia, E. Jee, Y. S. Chung, D. H. Kim, D. Choi, *Adv. Energy Mater.* **2019**, 9, 1803786.
- [36] Z. Lei, P. Wu, *Mater. Horiz.* **2019**, 6, 538.
- [37] Z. Lei, P. Wu, *Nat. Commun.* **2019**, 10, 3429.
- [38] Z. Cao, H. Liu, L. Jiang, *Mater. Horiz.* **2020**, 7, 912.
- [39] Y. Cao, T. G. Morrissey, E. Acome, S. I. Allec, B. M. Wong, C. Keplinger, C. Wang, *Adv. Mater.* **2017**, 29, 1605099.
- [40] L. Sun, S. Chen, Y. Guo, J. Song, L. Zhang, L. Xiao, Q. Guan, Z. You, *Nano Energy* **2019**, 63, 103847.
- [41] Y. Zhang, M. Li, B. Qin, L. Chen, Y. Liu, X. Zhang, C. Wang, *Chem. Mater.* **2020**, 32, 6310.
- [42] Y. Cao, Y. J. Tan, S. Li, W. W. Lee, H. Guo, Y. Cai, C. Wang, B. C.-K. Tee, *Nat. Electron.* **2019**, 2, 75.
- [43] J. Joseph, E. D. Jemmis, *J. Am. Chem. Soc.* **2007**, 129, 4620.
- [44] M. N. Garaga, M. Nayeri, A. Martinelli, *J. Mol. Liq.* **2015**, 210, 169.
- [45] O. Russina, A. Triolo, L. Gontrani, R. Caminiti, D. Xiao, L. G. Hines Jr., R. A. Bartsch, E. L. Quitevis, N. Plechkova, K. R. Seddon, *J. Phys.: Condens. Matter* **2009**, 21, 424121.
- [46] Y. Chen, H. Zhao, J. Mao, P. Chirarattananon, E. F. Helbling, N.-s. P. Hyun, D. R. Clarke, R. J. Wood, *Nature* **2019**, 575, 324.
- [47] X. Kang, C. Pan, Y. Chen, X. Pu, *RSC Adv.* **2020**, 10, 17752.
- [48] S. Niu, S. Wang, L. Lin, Y. Liu, Y. S. Zhou, Y. Hu, Z. L. Wang, *Energy Environ. Sci.* **2013**, 6, 3576.
- [49] V. Amoli, J. S. Kim, S. Y. Kim, J. Koo, Y. S. Chung, H. Choi, D. H. Kim, *Adv. Funct. Mater.* **2020**, 30, 1904532.
- [50] J.-Y. Sun, X. Zhao, W. R. Illeperuma, O. Chaudhuri, K. H. Oh, D. J. Mooney, J. J. Vlassak, Z. Suo, *Nature* **2012**, 489, 133.
- [51] W. J. Song, Y. Lee, Y. Jung, Y.-W. Kang, J. Kim, J.-M. Park, Y.-L. Park, H.-Y. Kim, J.-Y. Sun, *Sci. Adv.* **2021**, 7, eabg9203.
- [52] H. Yuk, T. Zhang, G. A. Parada, X. Liu, X. Zhao, *Nat. Commun.* **2016**, 7, 12018.
- [53] C. J. Thrasher, Z. J. Farrell, N. J. Morris, C. L. Willey, C. E. Tabor, *Adv. Mater.* **2019**, 31, 1903864.
- [54] K. Dandekar, B. I. Raju, M. A. Srinivasan, *J. Biomech. Eng.* **2003**, 125, 682.
- [55] K. Amano, N. Goda, S. y. Nishida, Y. Ejima, T. Takeda, Y. Ohtani, *J. Neurosci.* **2006**, 26, 3981.